Publishing House
AKAPIT

COMPUTER METHODS IN MATERIALS SCIENCE

Informatyka w Technologii Materiałów

Vol. 7, 2007, No. 3

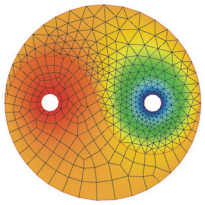

COMPARISON OF MATHEMATICAL MODELS FOR THE TURBULENT FLUID FLOW, HEAT TRANSFER AND SOLIDIFICATION IN THE CONTINUOUS CASTING PROCESS

RODRIGO OTTONI DA SILVA PEREIRA, ROBERTO PARREIRAS TAVARES

Federal University of Minas Gerais, Belo Horizonte, Brazil
Corresponding author: rtavares@demet.ufmg.br (R. Tavares)

Abstract

In the present work a mathematical model for the continuous casting process and its principal phenomena was developed. The model takes into account: heat transfer, fluid flow and mass transfer. The model allows the calculation of temperature, velocity, carbon concentration and turbulence variables profiles; and the variation of the solidified shell thickness along the caster. The new features of the present model are the inclusion of the effects of nozzle port configuration on the fluid flow and the possibility to perform calculations for the entire casting length. The effect of fluid flow and segregation was evaluated and it was shown that the mathematical model should take the fluid flow into account and that segregation has a minor effect in the temperature and fluid flow profiles. The introduction of the effect of segregation in the model indicates that the carbon content is lower near the surface and higher in the center of the strand. The model also showed that the strand becomes completely solid at approximately 13m below the meniscus in the case studied. The fluid flow affects the process in the first 4 to 5 m of the strand, being important only in the first 2 m. Different nozzle port angles were simulated and it was shown that a port with a downward angle leads to lower turbulence at the meniscus level in the mould.

Key words:continuous casting, mathematical modelling, fluid flow, segregation, turbulence

1. INTRODUCTION

The continuous casting process is usually studied by means of physical and mathematical models, since experimental work with liquid steel is difficult. Considering the limitations of the physical models, especially in the study of solidification, mathematical modeling becomes an important tool for the study of the continuous casting process.

The objective of the present work is the development of a model for the continuous casting machine. This model should be as complete as possible, since most of the models found in literature take into account only some aspects of the process. Thomas et al (1990) developed a model whose focus was the fluid flow in the region of the mould. It was a bidimensional model using a high Reynolds number K–ε turbulence model. The solidified shell thickness was predetermined, the simulated caster length was 3m and the nozzle port angle was considered. Aboutalebi et al (1995) developed a bidimensional model using a low Reynolds number K–ε turbulence model. The model considered solidification and the segregation of carbon. The nozzle configuration was not considered. Liquid steel was supposed to enter the strand vertically and the simulated caster length was 3m. Yang et al (1998) developed a tridimensional model using a high Reynolds number K–ε turbulence model. Solidification and segregation of solutes were considered. The simulated caster length was 4m. The nozzle region was not simulated and the inlet jet was supposed to follow the nozzle port

 ISSN 1641-8581

angle. Qiu et al (2004) developed a tridimensional model using a low Reynolds number K–ε turbulence model. The focus of that investigation was the flow in the upper region of the strand. It considered solidification but did not incorporate segregation. Apparently, the simulated caster length was 14 m.

It has already been shown that the fluid flow has a great influence in the continuous casting process, so it should be taken into account. It affects the growth of the solidified shell as well as the flotation of inclusions. The present model takes into account the segregation of solutes during solidification. The model comprises equations for turbulent flow, heat transfer and mass transfer and solidification. The model also considers the nozzle port configuration and the calculations are performed for the whole strand, until it reaches the cutter.

After the development of the model, a series of simulations were performed. In these simulations, the effect of the incorporation of segregation was analyzed by comparing its predictions to the predictions of other versions of the model. Different nozzle port angles of the submerged entry nozzle (SEN) were simulated and their effect on the fluid flow and heat transfer studied in order to verify their effect on the process.

2. MATHEMATICAL MODEL

2.1. Assumptions

The following assumptions were made in the development of the model of the continuous casting machine:

- the problem is assumed to be at steady state with respect to a fixed coordinate system;
- the strand curvature is neglected;
- local thermodynamic equilibrium during solidification is assumed to prevail;
- liquid steel is considered as an incompressible Newtonian fluid and turbulence effects are approximated using a low Reynolds number K–ε turbulence model;
- shrinkage of the liquid steel during solidification is neglected;
- solid phase is rigid and moves with a prescribed velocity (casting speed);
- the free surface of steel is flat and kept at a constant level;
- the carbon steel considered in this study was assumed to be a binary Fe-C alloy;
- the latent heat of δ-γ transformation is neglected;
- heat generation by viscous dissipation is negligible;
- the effects of surface tension gradients at the free surface arising from temperature and/or concentration gradients (thermo-diffusion capillarity) are negligible;
- mushy zone has columnar dendritic morphology and behaves as a porous media, where the solid-liquid interaction can be quantified using Darcy's law. Pore formation is ignored;
- under-cooling (thermal, constitutional) is negligible. The tip of the columnar dendrites is located at the liquidus isotherm.

The model comprises the mould and the secondary cooling regions. The model considers symmetry along the width and the thickness of the slab. The model also includes the region of the submerged entry nozzle.

2.2. Mathematical Formulation

In the development of the conservation equations, the continuum model suggested by Bennon and Incropera (1987) was adopted. This *continuum* formulation has been shown to provide realistic predictions for phase change problems (Prescott et al, 1991) and to yield equations that have the same form as those appearing in single phase flows. This certainly facilitates their solution using relatively well established procedures (Patankar, 1980).

Considering the assumptions that were enunciated in the previous section, and the additional approximation of equal and constant densities of solid and liquid phases, the time-smoothed conservation equations for three-dimensional turbulent flows can be written in the form presented below.

Turbulence was taken into account by means of the two-equation K–ε model. Considering previous successful applications in solidification problems (Reza et al, 1995; Prescott and Incropera, 1995; Shyy et al, 1992; Farouk et al, 1992; Seyedein and Hasan, 1996), a low-Reynolds-number formulation of the K–ε model was adopted.

A complete list of variables is presented in the Appendix A.

Mass conservation (Continuity equation):

$$\nabla\left(\rho u_j\right) = 0 \tag{1}$$

Conservation of momentum (equations of motion):

$$\nabla(\rho u_j u_i) = \nabla(\mu_{eff} \nabla u_j) - \nabla P + \frac{\mu_l}{K_p}(u_i - u_{i,s}) + \rho g_i \beta_T (T - T_{ref}) + \sum_k \rho g_i \beta_{c,k} (C_k - C_{ref,k}) \quad (2)$$

where:

$$\mu_{eff} = \mu_l + \mu_t \quad (3)$$

$$\mu_t = \frac{C_\mu f_\mu \rho K^2}{\varepsilon} \quad (4)$$

$$C_\mu = 0.09 \quad (5)$$

$$f_\mu = e^{\left(\frac{-3.4}{\left(1+\frac{\mathrm{Re}_t}{50}\right)^2}\right)} \quad (6)$$

$$K_p = \frac{(f_l + 0.002)^3}{1.8x10^{10}(1 - f_l)^2} \quad (7)$$

The permeability (K_p) equation was proposed by Aboutalebi et al (1995). When f_l tends to zero, permeability tends to zero. To avoid a division by zero in the computer program when f_l is 0, a value of two thousandths was added to f_l in the numerator of K_p, in equation (7). This term would be significant only for small values of f_l , but in this case permeability would be almost zero (and velocity equals to solid velocity). When f_l tends to one, permeability becomes high and the term that is function of permeability in equation (2) tends to zero.

Conservation of the turbulent kinetic energy:

$$\nabla(\rho K u_j) = \nabla\left(\frac{\mu_t}{\sigma_K} \nabla K\right) + G_K - \rho\varepsilon + D_K + A_K K \frac{(1 - f_l^2)}{(f_l + 0.002)^3} \quad (8)$$

where:

$$G_K = \mu_t \sum\sum \left[\frac{\partial u_i}{\partial x_j}\left(\frac{\partial u_j}{\partial x_i} + \frac{\partial u_i}{\partial x_j}\right)\right] \quad (9)$$

$$D_K = 2\frac{\mu_l}{\rho} \sum \left(\frac{\partial \sqrt{K}}{\partial x_i}\right)^2 \quad (10)$$

$$\sigma_K = 1.0 \quad (11)$$

A value of 1x 10^6 was assigned to A_K , as suggested by Aboutalebi et al (1995).

Conservation of the turbulent energy dissipation rate:

$$\nabla(\rho \varepsilon u_j) = \nabla\left(\frac{\mu_t}{\sigma_\varepsilon} \nabla \varepsilon\right) + \frac{C_1 f_1 \varepsilon G_K}{K} - \frac{C_2 f_2 \rho \varepsilon^2}{K} + E_K + A_K \varepsilon \frac{(1 - f_l^2)}{(f_l + 0.002)^3} \quad (12)$$

where

$$f_1 = 1 \quad (13)$$

$$f_2 = 1 - 0.3e^{-\mathrm{Re}_t^2} \quad (14)$$

$$C_2 = 1.92 \quad (15)$$

$$C_1 = 1.44 \quad (16)$$

$$\sigma_\varepsilon = 1.0 \quad (17)$$

$$E_K = 2\frac{\mu_l \mu_t}{\rho} \sum \sum \left(\frac{\partial^2 u_i}{\partial x_j^2}\right)^2 \quad (18)$$

In equations (8) and (12), a value of two thousandths was added to f_l in the denominator of the term that takes into account the influence of solids.

Conservation of energy:

$$\nabla(\rho H u) = \nabla\left[\left(\frac{\mu_l}{\mathrm{Pr}_l} + \frac{f_l \mu_t}{\mathrm{Pr}_t}\right)\nabla H\right] + \nabla\left[\left(\frac{\mu_l}{\mathrm{Pr}_l} + \frac{f_l \mu_t}{\mathrm{Pr}_t}\right)\nabla(H_s - H)\right] - \nabla\left[f_s \rho (u_j - u_{j,s})(H_l - H_s)\right] \quad (19)$$

where

$$\mathrm{Pr}_t = 1.0 \quad (20)$$

Conservation of species (carbon):

$$\nabla(\rho C u) = \nabla\left[\left(\frac{\mu_l}{Sc} + \frac{f_l \mu_t}{Sc_t}\right)\nabla C\right] + \nabla\left[\left(\frac{\mu_l}{Sc} + \frac{f_l \mu_t}{Sc_t}\right)\nabla(C_l - C)\right] - \nabla\left[f_s \rho (u_j - u_{j,s})(C_l - C_s)\right] \quad (21)$$

where:

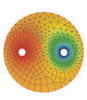

$$Sc_t = 1.0 \tag{22}$$

In the mushy zone, velocities are calculated by (Yang et al, 1998):

$$u = u_s f_s + u_l f_l \tag{23}$$

To evaluate the fraction of solids in the mushy zone, equation (24), proposed by Yang et al (1998), is used.

$$f_s = \frac{1}{1-k_{sl}} \frac{T - T_{liq}}{T - T_m} \tag{24}$$

where k_{sl} is calculated by the following equation:

$$k_{sl} = \frac{C_s}{C_l} \tag{25}$$

In the study of segregation, equation (26) was used. The values of k_{sl} were estimated from the iron-carbon phase diagram. For carbon contents lower than 0.2%, k_{sl} is 0.192 and, for carbon contents greater than 0.2%, k_{sl} is 0.465.

$$C_l = \frac{C}{(1-f_s)+k_{sl} f_s} \tag{26}$$

Boundary conditions

Before solving the conservation equations, boundary conditions for the different dependent variables have to be specified. In the specification of these conditions, symmetry was considered and the solution domain corresponds to only one quarter of the caster. The solution domain is schematically represented in Figure 1.

Inlet of liquid metal

At the inlet, the three velocity components, temperature and carbon concentration were prescribed. Velocity is determined through mass conservation based on casting speed and the cross section of the strand. The turbulent kinetic energy and the rate of dissipation of turbulent energy at the inlet are estimated using the following correlations found in the literature (Yeh et al, 1994; Chen and Pehlke, 1996; Joo and Guthrie, 1993). These correlations are usually expressed in terms of the dimensions of the nozzle used to feed the liquid metal into the caster and of the inlet velocity.

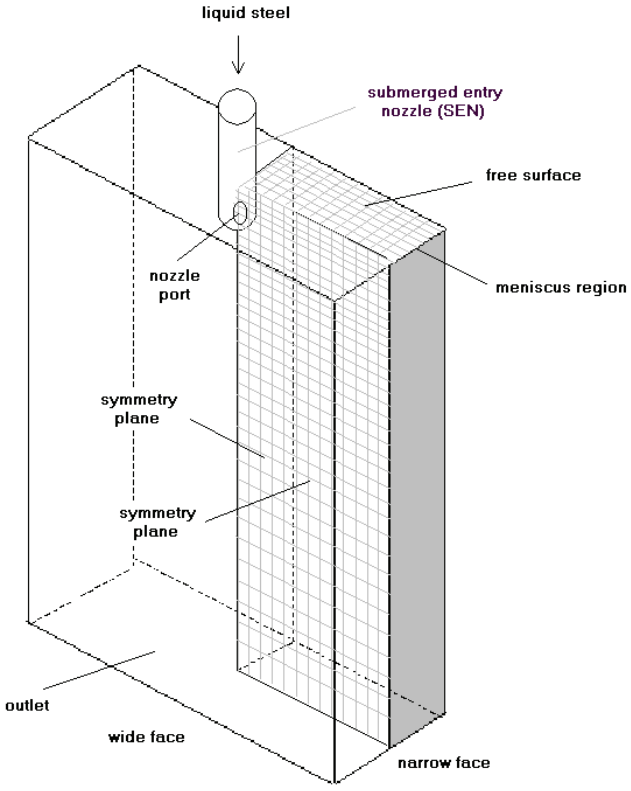

Fig. 1. *Solution domain for the mathematical model of the continuous casting machine.*

$$K_{in} = 0.01 u_{in}^2 \tag{27}$$

$$\varepsilon_{in} = \frac{K_{in}^{1.5}}{R_{noz}} \tag{28}$$

where:
u_{in} = inlet velocity;
R_{noz} = submerged entry nozzle radius.

Walls

At the walls, all velocities and turbulence variables were set to zero. At the mold walls, the velocity in the casting direction was set to the casting speed.

Heat transfer within the nozzle walls was not analyzed. At the interface of the walls and the liquid steel, an adiabatic condition was assumed.

Free surface

The velocity components and gradients of all the other variables, except temperature, normal to the free surface were set equal to zero.

In terms of heat transfer, heat losses due to convection and radiation were considered.

Symmetry planes

The velocity components and gradients of all the other variables, except temperature, normal to the symmetry planes were set equal to zero.

Outlet

At the exit of the caster, fully developed flow was assumed. This implies that the normal gradients of all variables are zero at the outlet. Velocity in the casting direction is equal to the casting speed.

For the heat transfer in the mould, equation (29) is used. This correlation was extracted from graphs in the literature (Schwerdtfeger, 2003). In this equation, the heat flux varies with the distance to the meniscus. The heat flux is also varied according to the position along the width and the thickness of the strand. The heat flux is maximum at the center of the faces and decreases linearly towards the corner, where the heat flux is 80% of that at the center, as proposed by Yang et al (1998).

$$q = 1.732 \cdot 10^6 \, e^{(-1.155 \cdot d_m)} \tag{29}$$

where:
q = heat flux, in W/m^2;
d_m = distance below meniscus, in m.

The heat transfer coefficient in the secondary cooling zone was estimated using the following equation, proposed by Brimacombe and Batista (1984):

$$h = 7.08 \times 10^5 \left(W_a\right)^{0.75} \left(T_{\text{sup}}\right)^{-1.2} + 116 \tag{30}$$

where:
h = heat transfer coefficient, in W/m^2·K;
W_a = water flow in sprays, in l/m^2·s;
T_{sup} = surface temperature of the strand, in K.

This heat transfer equation was also modified in order to vary with width and thickness. The heat transfer coefficient at the corner is assumed to be 40% of that in the middle of the wide face and the heat transfer coefficient in the narrow face is assumed to be the same as that at the corner, as proposed by Yang et al (1998).

Steel properties

Steel density (solid and liquid) was considered equal to 7000 kg/m^3. Liquid steel viscosity is equal to 6.2x10^{-3} kg/m.s. Latent heat of fusion of steel was considered equal to 270000 J/kg.

The thermal conductivity of steel, in W/m.K, is calculated by the following equations, presented by Brimacombe et al (1984):

$$k_{steel} = 64.1354 - 0.0427 T_{steel} \quad for \quad T_{steel} < 870^o C \tag{31}$$

$$k_{steel} = 16.9952 + 0.0115 T_{steel} \quad for \quad T_{steel} > 870^o C \tag{32}$$

In these equations, temperature is in Celsius.

The specific heat of steel, in J/kg.K, is calculated by the following equations:

$$C_{p\,steel} = 2368 - 14.92 T_{steel} + 4.107x10^{-2}\left(T_{steel}\right)^2 - 4.696x10^{-5}\left(T_{steel}\right)^3 + 1.953x10^{-8}\left(T_{steel}\right)^4 \quad for\ T_{steel} \le 1020K \tag{33}$$

$$C_{p\,steel} = 7802 - 5.278 T_{steel} - 3.676x10^{-3}\left(T_{steel}\right)^2 + 1.388x10^{-6}\left(T_{steel}\right)^3 + 1.031x10^{-9}\left(T_{steel}\right)^4 \quad for\ 1020K < T_{steel} \le 1210K \tag{34}$$

$$C_{p\,steel} = 703 \quad for\ T_{steel} > 1210K \tag{35}$$

These expressions were proposed by Suzuki et al (2001).

The emissivity of liquid steel was set to 0.28. The emissivity of solid steel is calculated by a regression equation based on data presented by Ingerslev and Henein (1997).

$$\varepsilon_{steel} = 0.627 + 1.981 \cdot 10^{-4} T_{steel} \tag{36}$$

In this equation, temperature is in Celsius.

2.3. Numerical procedure

In the present study, the in-house METFLO code (Aboutalebi, 1994) was adapted to solve the conservation equations. The governing equations were discretized using a fixed-grid control-volume-based finite difference scheme and solved using a single domain numerical solution procedure. The velocity-pressure coupling in the momentum conservation equations is handled using the SIMPLER algorithm (Patankar, 1980). The algebraic equations were solved using an alternating-direction line-by-line

method (TDMA method). To guarantee convergence, under-relaxation was applied to the variables and source terms. It was required that the summation of the residuals of all equations for each variable to be smaller than 0.2% before the numerical procedure was declared terminated.

The formulation proposed by Bennon and Incropera (1988) was used in the evaluation of the source terms of the energy and carbon conservation equations.

3. RESULTS AND DISCUSSION

In the present work a mathematical model for the continuous casting machine was developed. The model allows the calculation of the velocity and temperature profiles and the thickness of the solidified shell along the strand, so it can be a useful tool to study the continuous casting process. First simulations with different nozzle port angles were made to evaluate the effect of the nozzle port angle on the process. Then different models for the continuous casting machine, with different degrees of complexity, were compared in order to evaluate the advantages and limitations of each model. The first model neglects the effect of fluid flow and segregation, the second model neglects the effect of segregation taking into account the fluid flow, and the third model takes into account the fluid flow and segregation.

The simulations considered casting of a carbon steel (0.8%C) with a superheat of 30°C and a casting speed of 0.85 m/min.

3.1. Effect of Nozzle Port Angle

The nozzle port angle is an important parameter since it affects turbulence levels at the meniscus region and the heat load at the mould walls. Higher levels of turbulence can lead to a more significant entrainment of mould flux in the liquid steel and a greater heat load at the mould wall can damage the mould wall and shorten its life.

Different SEN port angles were simulated to verify their effect on the fluid flow and solidified shell thickness. The following angles were simulated: -20°, 0° and 20°. A negative angle means an upward port. In these simulations, only the first 7m of the continuous casting machine were simulated, since prior simulations have shown that the SEN port angle affect the fluid flow and the temperature profiles only in the upper part of the continuous casting machine. The simulations used a non-uniform grid with approximately 260,000 nodes. The conditions of the simulations are presented in Table 1. These simulations were run with the second model mentioned above, since its results are similar to those of the third model in terms of fluid flow and solidified shell thickness and it converges faster.

Table 1. *Conditions considered in the casting simulations for the study of the effects of nozzle port angle.*

Length of mold region in contact with the steel (m)	0.670
Length of secondary cooling zone 1 (m)	0.500
Length of secondary cooling zone 2 (m)	4.330
Length of secondary cooling zone 3 (m)	1.475
Slab width (m)	1.255
Slab thickness (m)	0.200
Submerged entry nozzle penetration depth (m)	0.150
Submerged entry nozzle internal diameter (m)	0.040
Submerged entry nozzle inlet height (m)	0.060
Submerged entry nozzle wall thickness (m)	0.0275
Water flow rate in cooling zone 1 ($l/m^2.s$)	3.00
Water flow rate in cooling zone 2 ($l/m^2.s$)	0.82
Water flow rate in cooling zone 3 ($l/m^2.s$)	0.42
Steel inlet temperature (°C)	1482
Liquidus temperature (°C)	1452.6
Solidus temperature (°C)	1365.6
Ambient temperature (°C)	25
Casting speed (m/s)	0.0142
Steel throughput (tons/h)	89.6

Figure 2 shows the velocity profiles at the symmetry plane along the width of the caster for the upper regions of the continuous casting machine for the three nozzle port angles. It can be seen that there are two recirculation zones: one above and the other, approximately 1m long, below the inlet jet. When the nozzle port angle is –20°, the upper recirculation zone almost disappears and the center of the inlet jet reaches the wall approximately 15 cm below the meniscus. For the nozzle port angles of 0° and 20°, the center of the inlet jet reaches the wall 20 and 30 cm below the meniscus, respectively. If the inlet jet followed the nozzle port angle, it would reach the wall 12 and 23 cm above the meniscus level for the nozzle port angles of 0° and 20°, respectively. For the nozzle port angle of –20°, the inlet jet would be directed to the surface of the liquid steel in the mould. The inlet jet does not exactly follow the nozzle port angle. This can also be confirmed by the pressure profile in the center of the narrow face of

the mould, presented in Figure 3. These results also indicate that the differences in the velocity profiles for the different nozzle port angles virtually disappear for distances superior than 2m below the meniscus.

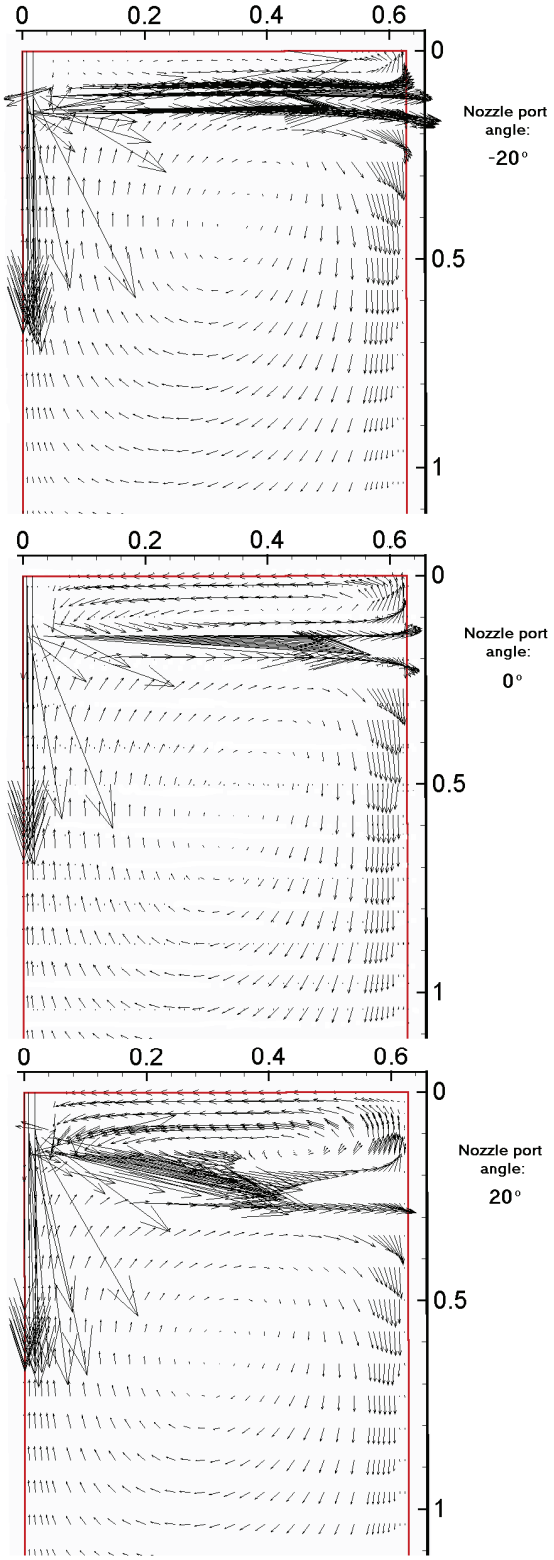

Fig. 2. *Velocity profiles at the symmetry plane along the narrow face in the upper region of the continuous casting machine for different nozzle port angles.*

The solid shell thicknesses in the narrow and in the wide faces of the mould for the different nozzle port angles are presented in Figures 4 and 5, respectively. The solid shell thickness is not significantly affected by the nozzle port angle.

The temperature profiles are affected by the nozzle port angle in the upper region of the caster, as shown in Figure 6. As the nozzle port angle increases (and the nozzle port is more directed downwards), the isotherm corresponding to 1452.6°C (liquidus temperature) tends to reach the lower levels of the strand.

Another relevant parameter is the kinetic energy of turbulence (K). Higher levels of the kinetic energy of turbulence, particularly in the meniscus region, lead to fluctuations of the liquid steel level in the mould and increase the risk of entrainment of mould flux. Figure 7 presents the variation of the kinetic energy of turbulence at the free surface for the three different nozzle port angles. The levels of turbulence and the risk of mould powder entrainment tend to decrease as the angle of the port increases (downward port).

The temperature levels at the free surface near the meniscus are also relevant, since freezing at the free surface can lead to quality problems. Figure 8 shows the temperature profiles at the free surface, for the different nozzle port angles. It can be seen that the temperatures are slightly above the liquidus temperature (1452.6°C) for the three cases. The differences among the cases are small, but it seems that the risk of meniscus freezing would be lower for a nozzle port angle of 20°, since the area at a temperature next to the liquidus temperature is smaller for that case.

3.2. Comparison of Different Models

The first mathematical models for the continuous casting process considered only heat transfer and solidification. Turbulent fluid flow and segregation were neglected in these models.

The objective in this part of the study is to analyze the effects of incorporating fluid flow and segregation in the heat transfer and solidification model. As mentioned previously, three different models were developed.

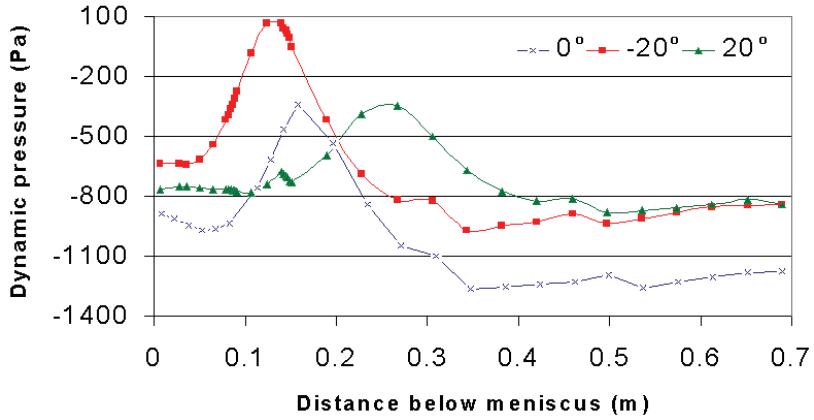

Fig. 3. Variation of dynamic pressure in the center of narrow face of the mould for different nozzle port angles.

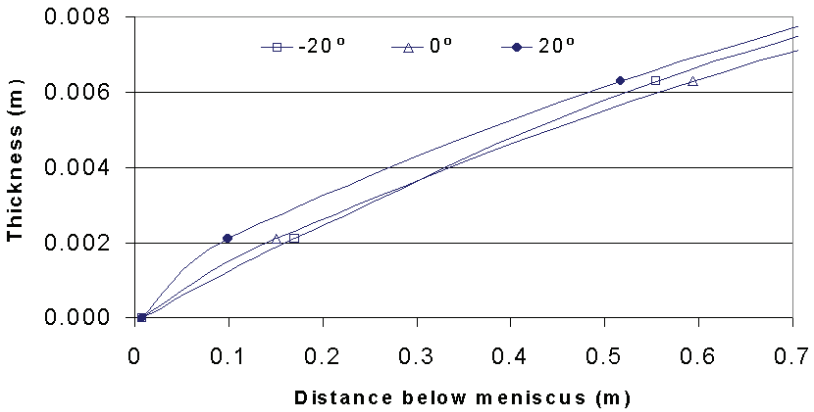

Fig. 4. Solid shell thickness variation at the symmetry plane along the narrow face of the mould for different nozzle port angles.

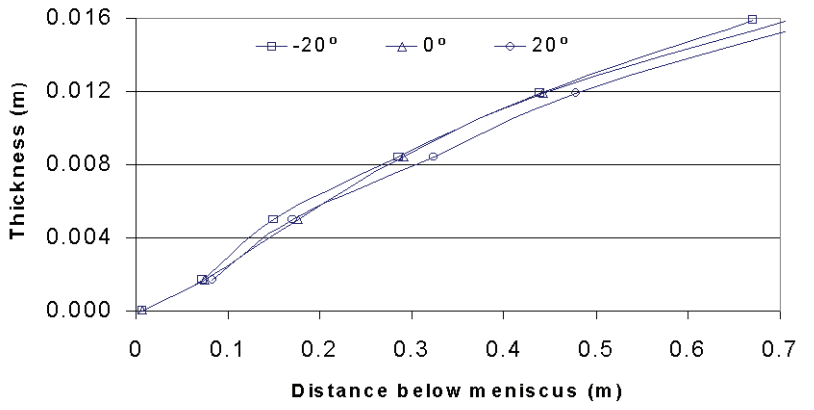

Fig. 5. Solid shell thickness variation at the symmetry plane along the wide face of the mould for different nozzle port angles.

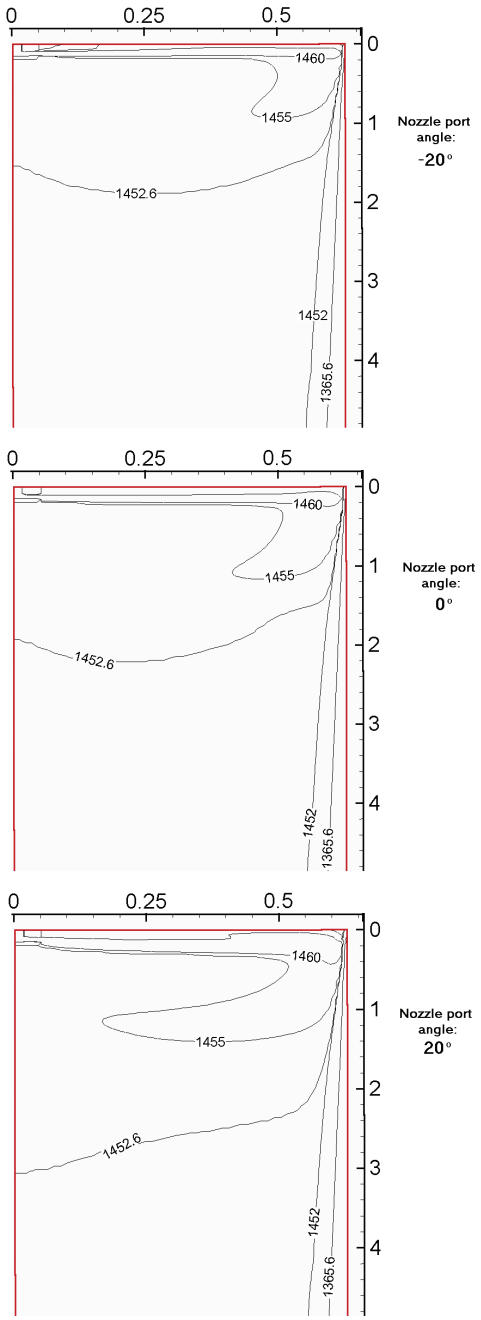

Fig. 6. Temperature profiles at the symmetry plane along the narrow face in the upper region of the continuous casting machine for different nozzle port angles.

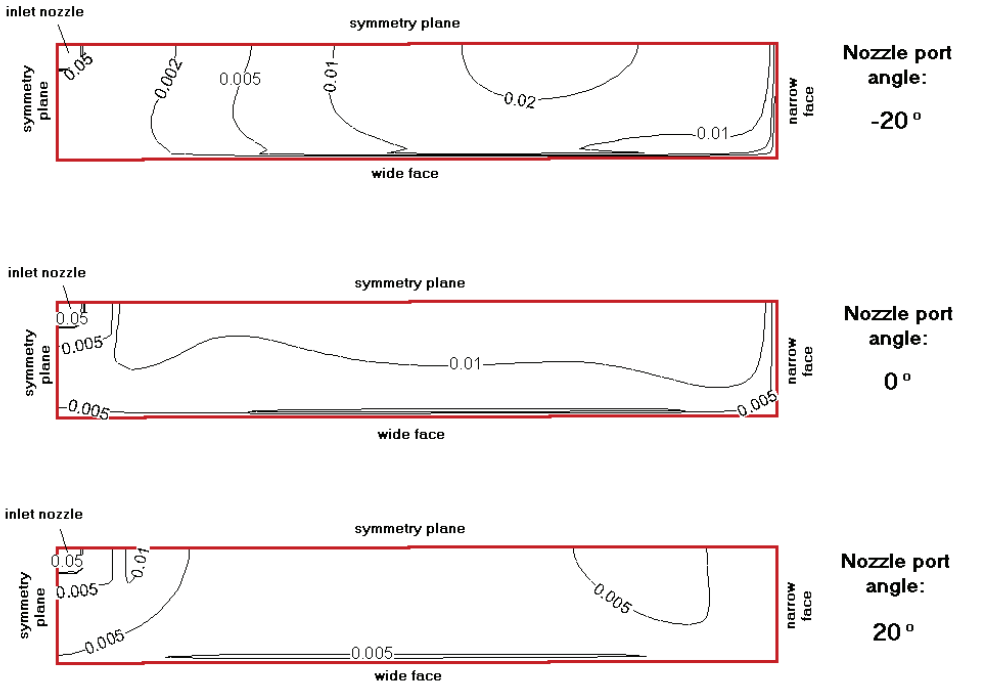

Fig. 7. *Profiles of kinetic energy of turbulence at the free surface for different nozzle port angles.*

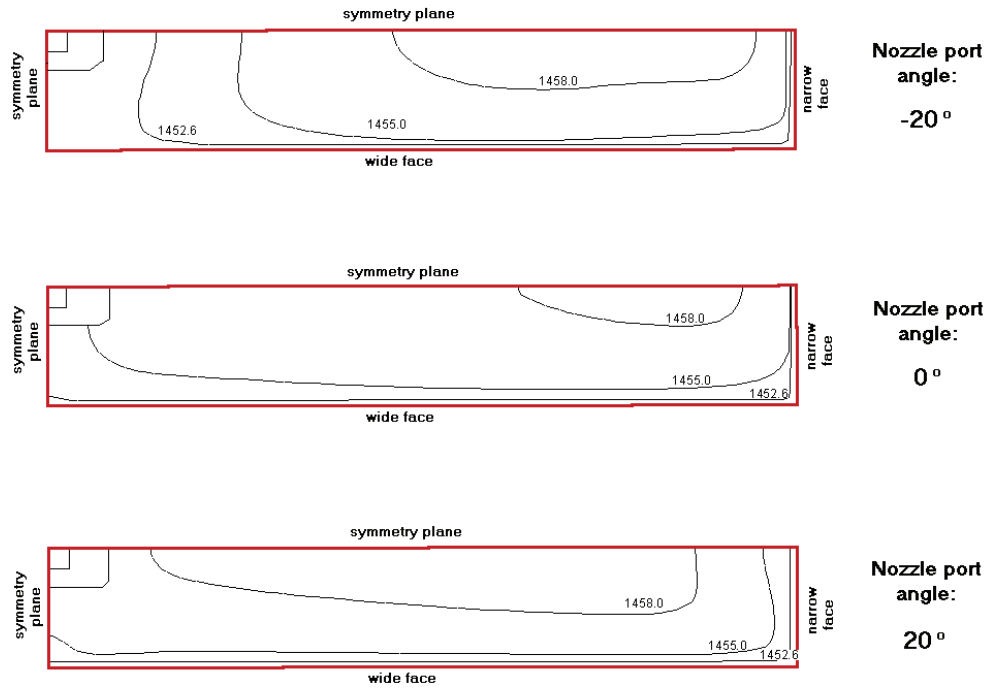

Fig. 8. *Temperature profiles at the free surface for different nozzle port angles.*

The first model includes only heat transfer and solidification and adopts the approach described by Brimacombe (1984). In this model, the transient temperature distribution in a bidimensional slice of the slab is calculated as it moves along the caster at the casting speed. In this case, each time corresponds to a different distance to the meniscus. The second and third models are tridimensional models, described in section 2 of the present work, and consider fluid flow, heat transfer and solidification. The third model considers also carbon segregation. The second model allows the calculations of temperature, velocity and turbulence variables profiles, and the third model also calculates the carbon concentration profiles. The simulations for the second and third models used a non-uniform grid with 540,000 nodes, approximately. The conditions considered in the simulations are presented in Table 2.

For an initial guess assuming all velocities equal to zero, K and ε equivalent to 1% of the correspondent inlet values and temperatures equal to that of the inlet, converged solutions were obtained after 40000 iterations. This number was reduced when a preconverged solution was used as an initial guess. Each iteration took approximately 1.2 min on a 2 GHz computer with 1 Gbyte RAM memory.

The solidified shell should be strong enough to stand the ferrostatic pressure. Since the strength of the shell is related to its thickness, it is important to evaluate the shell thickness along the caster.

Table 2. *Casting conditions considered in the simulations.*

Length of mould region in contact with the steel (m)	0.670
Length of secondary cooling zone 1 (m)	0.500
Length of secondary cooling zone 2 (m)	4.330
Length of secondary cooling zone 3 (m)	3.810
Length of secondary cooling zone 4 (m)	4.110
Slab width (m)	1.255
Slab thickness (m)	0.200
Submerged entry nozzle penetration depth (m)	0.150
Submerged entry nozzle internal diameter (m)	0.040
Submerged entry nozzle inlet height (m)	0.060
Submerged entry nozzle port angle	0^o
Submerged entry nozzle wall thickness (m)	0.0275
Water flow rate in cooling zone 1 ($l/m^2.s$)	3.00
Water flow rate in cooling zone 2 ($l/m^2.s$)	0.82
Water flow rate in cooling zone 3 ($l/m^2.s$)	0.42
Water flow rate in cooling zone 4 ($l/m^2.s$)	0.29
Carbon in steel (%)	0.80
Steel inlet temperature (^oC)	1482
Ambient temperature (^oC)	25
Casting speed (m/s)	0.0142
Steel throughput (t/h)	89.6

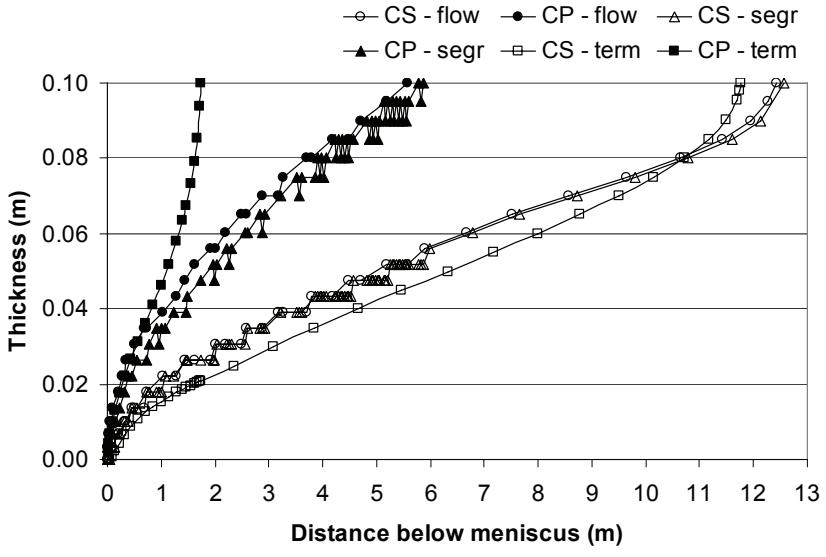

Fig. 9. *Comparison of shell thickness in the symmetry plane at the wide face along the strand for the different models.*

The thickness of the mushy zone and solidified shell in the wide face for the three models are compared in Figure 9. The mushy zone thickness is identified by CP and the solidified shell by CS. The first model is identified by *term,* the second by *flow* and the third by *segr*. The solidified shell thickness is almost the same for the second and third models, but for the first model it is thinner in the upper part of the strand and thicker in the end of the continuous casting machine. The mushy zone in the first model is significantly thicker than in the other two models and the mushy zone in the second model is a little thicker than in the third model. The difference in the mushy zone thickness between the second and the third models can be explained by a higher carbon concentration near the solidification front in the third model, which reduces the liquidus temperature. The differences between the first and the other two models are related to the fluid flow that is not considered in the first model. The oscillation in the mushy zone curve for the third model is due to a small instability in the numerical procedure.

Regarding these oscillations, it was observed that it is due to the strong coupling of the thermal and carbon concentration fields. If the underrelaxation factors for the temperature and carbon concentration equations are reduced, the oscillations eventually disappear, but the computation time to achieve convergence is significantly increased and the results are virtually the same.

The thickness of the solidified shell and mushy zone in the strand at the exit of the mould are presented in Figure 10. It can be seen that the solidified shell is thicker in the wide face than in the narrow face and that the results for the second and third models are similar in terms of solidified shell thickness. It can also be observed that the mushy zone is thicker in the wide face than in the narrow face and that the second model indicates a thicker mushy zone compared to the third model.

The temperature profiles in the symmetry plane for the second and third models are presented in Figures 11 and 12. At the right side a detailed view of the upper region of the caster is presented for each graph. The temperature profiles in the two cases are similar, but some differences can be noted in the upper part of the strand. There is an extra isotherm line for the temperature of 1452.6^oC, which is the liquidus temperature for the second model, and the distances between the isotherms for 1455 and

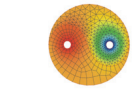

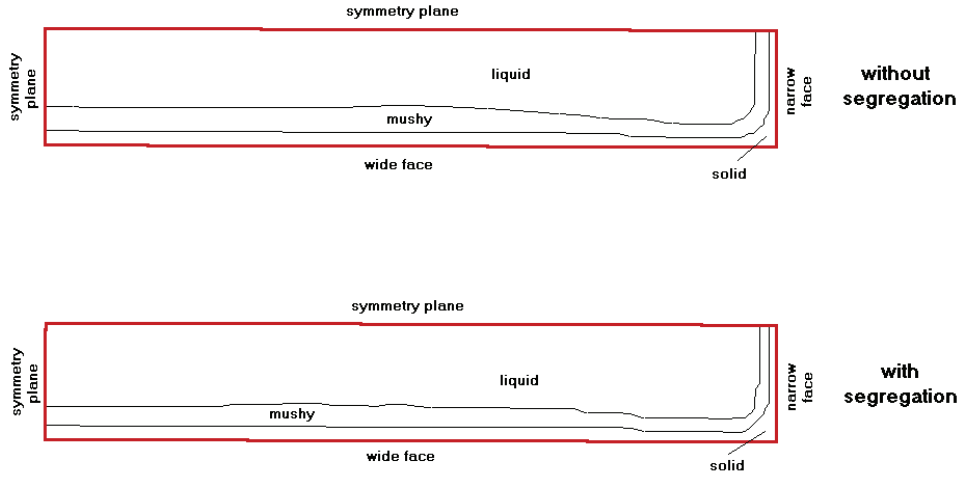

Fig. 10. *Solidified shell and mushy zone thickness at the exit of the mould for the second and third models.*

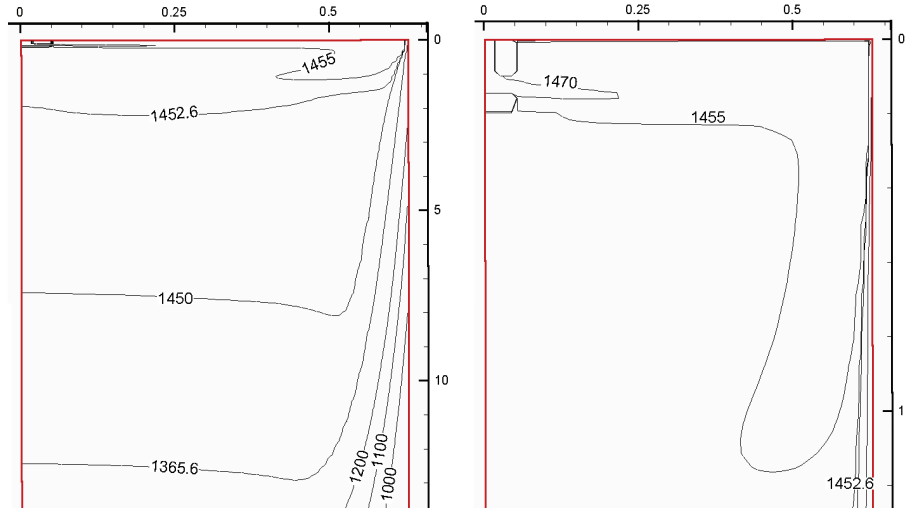

Fig. 11. *Temperature profile at the symmetry plane for the second model (without segregation, liquidus temperature = 1452.6°C and solidus temperature = 1365.6°C).*

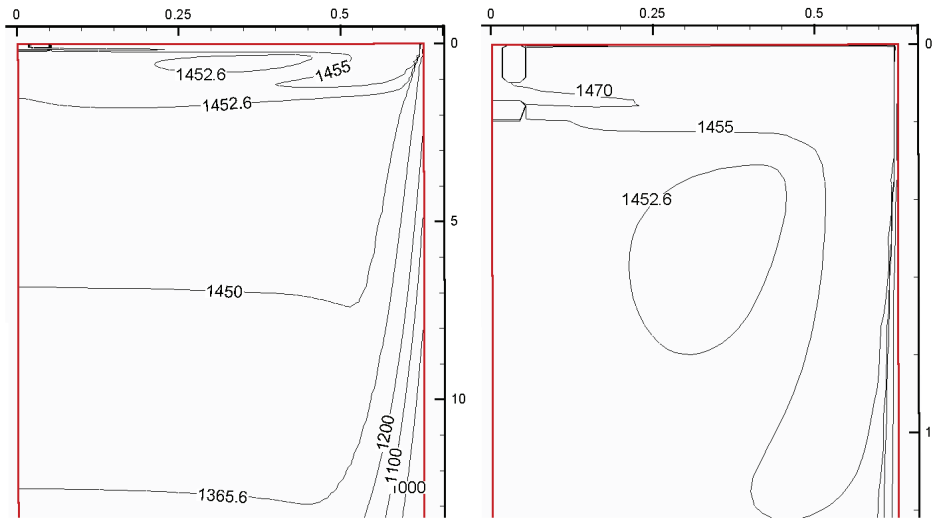

Fig. 12. *Temperature profile at the symmetry plane for the third model (with segregation).*

1452.6°C are clearly different. These differences can be explained by the different liquidus and solidus temperatures, which vary according to the carbon content for the third model and causes differences in the thickness of the mushy zone.

The temperature profiles in the center of the wide face along the strand for the three models are presented in Figure 13. These curves show that the heat withdrawal is greater in the mold region. When the cooling conditions are changed, there are significant changes in the curve inclination (0.7m, 1.2m, 5.5m and 9.3m below meniscus). As the cooling conditions become weaker, the slope of the curve decreases. The results for the second and third models are almost the same, confirming that the temperature predictions for these models are close to each other. In the first model, due to the fact that the fluid flow is neglected, the temperature distribution across the cross section of the strand becomes completely different, especially in the mould region.

The second model assumes a constant carbon concentration throughout the strand. The third model calculates the carbon concentration in the strand based on a conservation equation. This is the major difference be-

tween the second and third models. Figure 14 presents the dimensionless carbon concentration, which is defined as the actual concentration divided by the nominal concentration, in the solidified slab according to the model including segregation. Due to symmetry, only a quarter of the strand is shown. The carbon concentration is lower near the surface, especially close to the corner. The carbon concentration is higher in the center of the slab, which is the last region to solidify. The fact that most of the cross section of the strand has a dimensionless carbon concentration close to 1.0 explains why the results of the second and third models are similar.

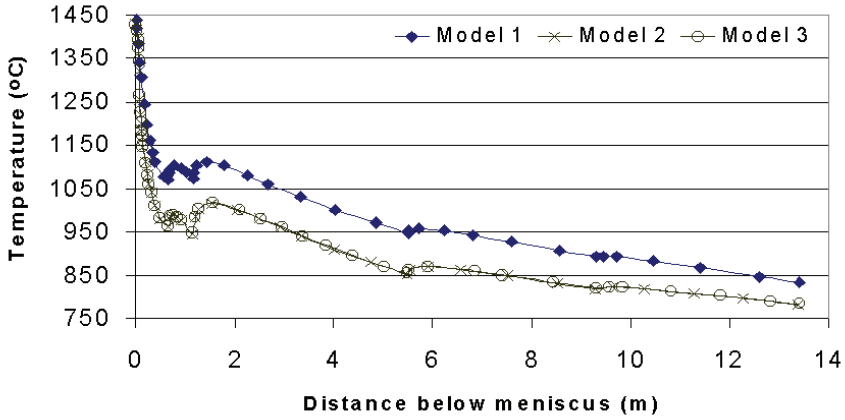

Fig. 13. *Comparison of temperature variation in the symmetry plane at the wide face along the strand for the different models.*

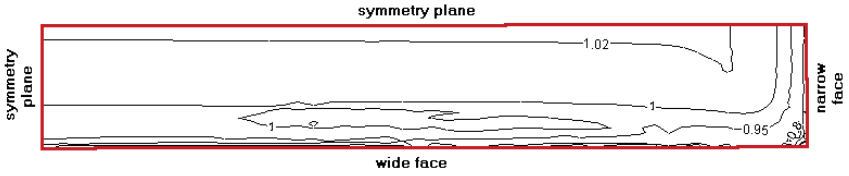

Fig. 14. *Dimensionless carbon concentration in the solidified slab according to the model with segregation.*

4. SUMMARY AND CONCLUSIONS

In the present work, a steady-state three-dimensional turbulent fluid flow, heat and mass transfer (segregation) model for continuous casting of slabs has been developed. For turbulence, a low Reynolds number form of the K–ε model has been used. The model includes the nozzle used to deliver liquid metal into the caster and also the possibility to perform calculations for the entire caster length. The METFLO code (Aboutalebi, 1994) was adapted to solve the conservation equations. The governing equations were discretized using a fixed-grid control-volume-based finite difference scheme and solved using a single domain numerical procedure.

The mathematical model was used to evaluate the effects of the nozzle design, particularly the port angle, on the fluid flow and heat transfer in the caster. The predictions of the model were also compared to results obtained with simpler models, one neglecting the segregation effects and the other considering only heat transfer and solidification.

The simulations indicated that the angle of the nozzle ports does not have a significant effect on the variation of the solid shell thickness along the length of the caster. The temperature and the kinetic energy of turbulence levels, particularly at the free surface, are strongly affected by the port angles. Temperatures at the free surface tend to increase when a port with negative angle (upward) is used. This reduces the risk of meniscus freezing that can cause quality problems on the surface of the slab. However, the negative angle also leads to more intense turbulence at the free surface. This can have a negative effect on the quality of the product, not only due to the fluctuations of the liquid level in the mould, but also due to entrainment of mould flux.

The predictions of the mathematical model presented in this work were also compared to those of two simpler models, one neglecting segregation and the other considering only heat transfer and solidification. The results indicated that the predictions of the models, in terms of variation of the solidified shell thickness along the caster, are similar. In terms of fluid flow pattern, the results obtained with the models with and without segregation were virtually identical, with small differences in the locations and sizes of the recirculation zones. This indicates that models neglecting the effects of segregation can be used with confidence to predict fluid flow and heat transfer in continuous casting machines.

The model including segregation is more time consuming than the other models and should only be used when segregation levels in the final product must be predicted, possibly to analyze the effects of electromagnetic stirring. In this case, the present model should be coupled to the solution of the Maxwell equations.

APPENDIX A

Nomenclature

C = concentration
C_k = concentration of component k
C_l = concentration in liquid phase
C_s = concentration in solid phase
$C_{ref,j}$ = reference concentration for the Boussinesq approximation
C_p = specific heat
ε_{steel} = emissivity of solid steel
f_l = liquid fraction in the mushy zone
f_s = solid fraction in the mushy zone
g = gravity
h = heat transfer coefficient
H = enthalpy
H_l = enthalpy in the liquid phase
H_s = enthalpy in the solid phase
k = thermal conductivity
k_{sl} = partition coefficient
K = turbulent kinetic energy
K_p = permeability of the mushy zone
P = pressure
Pr_l = Prandtl number
Pr_t = turbulent Prandtl number
q = heat flux
Re_t = turbulent Reynolds number
Sc = Schmidt number
Sc_t = turbulent Schmidt number
T = temperature
T_{steel} = steel temperature
T_{liq} = liquidus temperature
T_m = melting point of pure iron
T_{ref} = reference temperature for Boussinesq approximation
u = velocity
u_i = velocity in direction i (i = x , y, z)
u_l = liquid phase velocity
u_s = solid phase velocity
x_i ,x_j = coordinates
$\beta_{c,k}$ = Boussinesq coefficient for concentration of component k
β_T = Boussinesq coefficient for temperature
ε = rate of dissipation of kinetic energy of turbulence
μ_{eff} = effective viscosity
μ_l = laminar viscosity
μ_t = turbulent viscosity
ρ = density

REFERENCES

Aboutalebi, R., 1994, *Modelling of turbulent transport phenomena and solidification in continuous casting systems*, PhD thesis, McGill University, Montreal.

Aboutalebi, R., Hasan, M., Guthrie, R.I.L., 1995, Coupled turbulent flow, heat, and solute transport in continuous casting processes, *Metall. Mater. Trans. B*, 26B, 731-744.

Bennon, W.D., Incropera, F.P., 1987, Numerical analysis of binary solid-liquid phase change using a continuum model, *Int. J. Heat and Mass Transfer*, 30, 2161-70.

Bennon, W.D., Incropera, F.P., 1988, Numerical analysis of binary solid-liquid phase change using a continuum model, *Numerical Heat Transfer*, 13, 277-296.

Brimacombe, J.K., 1984, Design of continuous casting machines based on a heat-flow analysis: state-of-art review, in: Brimacombe, J.K., Samarasekera, I.V., Lait, J.E., *Continuous Casting: Heat Flow, Solidification and Crack Formation*, 2, Iron and Steel Society, Warrendale, 17-28.

Brimacombe, J.K., Batista, L.A., 1984, *Continuous Casting. Heat Flow, Solidification and Crack Formation*, Iron and Steel Society, Warrendale, 1, 109-123.

Brimacombe, J.K., Weinberg, F., Hawbolt, E.B., 1984, Formation of longitudinal, midface cracks in continuously-cast slabs. in: Brimacombe, J.K.; Samarasekera, I.V., Lait J.E., *Continuous Casting: Heat Flow, Solidification and Crack Formation*, 2, Warrendale, Iron and Steel Society, 215-227.

Chen, H.S., Pehlke, R.D., 1996, Mathematical modeling of tundish operation and flow control to reduce transition slabs, *Metall. Mater. Trans*. B, 27B, 745-756.

Farouk, B., Apelian, D., Kim, Y. G., 1992, A numerical and experimental study of the solidification rate in a twin-belt caster, *Metall. Mater. Trans*. B, 23B, 477-492.

Ingerslev, P., Henein, H., 1997, An integral boundary approach for 1- and 2-D modeling of ingot reheating and cooling, *Iron and Steelmaker*, 24, 5, 75-85.

Joo, S., Guthrie, R.I.L., 1993, Inclusion behavior and heat-transfer phenomena in steelmaking tundish operations: part I. Aqueous modeling, *Metall. Mater. Trans*. B, 24B, 755-765.

Lait, J.E., *Continuous Casting. Heat Flow, Solidification and Crack Formation*, Iron and Steel Society, Warrendale, 2, 17-28.

Patankar, S.V., 1980, *Numerical heat transfer and fluid flow*, Hemisphere Publishing Corporation, 197.

Prescott, P.J., Incropera, F. P., 1995, The effect of turbulence on solidification of a binary metal alloy with electromagnetic stirring, *Trans. ASME – J. Heat Transfer*, 117, 716-724.

Prescott, P. J., Incropera, F. P., Bennon, W. D., 1991, Modelling of dendritic solidification systems : reassessment of the continuum momentum equation, *Int. J. Heat and Mass Transfer*, 34, 9, 2351-2359.

Qiu, S., Liu, H., Peng, S., Gan, Y., 2004, Numerical analysis of thermal-driven buoyancy flow in the steady macro-solidification process of a continuous slab caster, *ISIJ Int*., 44, 1376-1383.

Samarasekera, I.V., Lait, J.E., *Continuous Casting. Heat Flow, Solidification and Crack Formation*, Iron and Steel Society, Warrendale, 2, 215-227.

Schwerdtfeger, K. J., 2003, *Heat Withdrawal in Continuous Casting of Steel, The Making, Shaping and Treating of Steel*, 11th Edition, Casting Volume, The AISE Steel Foundation Pittsburgh, 1-41.

Seyedein, S. H., Hasan, M., 1996, A 3-D numerical prediction of turbulent flow, heat transfer and solidification in a continuous slab caster for steel, *Computational Fluid Dynamics and Heat/Mass Transfer Modelling in the Metallurgical Industry*, eds, Argyropoulos, S. A., Mucciardi, F., 146-163.

Shyy, W., Pang, Y., Hunter, G.B., Wei, D.Y., Chen, M.-H., 1992, Modeling of turbulent transport and solidification during continuous ingot casting, *Int. J. Heat and Mass Transfer*, 35, 5, 1229-1245.

Suzuki, M., Yamaguchi, R., Murakami, K., Nakada, M., 2001, Inclusion particle growth during solidification of stainless steel, *ISIJ Int*., 41, 247-256.

Thomas, B.G., Mika, L.J., Najjar, F.M., 1990, Simulation of fluid flow inside a continuous slab-casting machine, *Metall. Trans. B*, 21B, 387-400.

Yang, H., Zhao, L., Zhang, X., Deng, K., Li, W., Gan, Y., 1998, Mathematical simulation on coupled flow, heat, and solute transport in slab continuous casting process, *Metall. Trans. B*, 29B, 1345-1356.

Yeh, J.L., Hwang, W.S., Chou, C.L., 1994, An improved fluid flow model for slab tundishes and its comparison with a full-scale water model, *Applied Mathematical Modelling*, 18, 39-45.

PORÓWNANIE MODELI MATEMATYCZNYCH DLA PRZEPŁYWU TURBULENTNEGO PŁYNU, TRANSPORTU CIEPŁA I KRYSTALIZACJI W PROCESIE CIĄGŁEGO ODLEWANIA

Streszczenie

W ramach pracy zbudowany został model matematyczny procesu ciągłego odlewania stali oraz głównych zjawisk zachodzących w tym procesie. Model uwzględnia transport ciepła, przepływ cieczy i transport masy. Pozwala on na obliczanie pól temperatury i prędkości oraz profili rozkładu stężenia węgla i turbulencji, a także zmian grubości warstwy zakrzepniętej wzdłuż krystalizatora. Nową cechą zaprezentowanego modelu jest uwzględnienie wpływu konfiguracji dysz na przepływ cieczy oraz możliwość wykonywania obliczeń dla całej długości krystalizatora. W pracy oszacowano wpływ przepływu cieczy na segregację składu chemicznego i wykazano, że przepływ cieczy powinien być uwzględniany przez model matematyczny COS, a wpływ segregacji na pola temperatury i na przepływ cieczy jest pomijalny. Wprowadzenie segregacji do modelu pokazuje, że stężenie węgla jest mniejsze w pobliżu powierzchni i większe w środku pasma. Model pokazuje również, że w badanym przypadku pasmo krzepnie w całej objętości w odległości około 13 m poniżej powierzchni cieczy. Przepływ cieczy ma wpływ na proces na początkowej długości 4 to 5 m, przy czym ten wpływ jest bardzo istotny tylko na początkowej długości około 2 m. W symulacjach uwzględniono różne możliwe kąty nachylenia dysz i wykazano, że układ ze zmniejszonym nachyleniem prowadzi do mniejszych turbulencji na poziomie menisku w kadzi.

Received: March 19, 2007
Received in a revised form: April 6, 2007
Accepted: September 3, 2007